Whitmarsh, R.B., Sawyer, D.S., Klaus, A., and Masson, D.G. (Eds.), 1996
Proceedings of the Ocean Drilling Program, Scientific Results, Vol. 149

41. DETAILED RELATIONSHIP BETWEEN TECTONICS AND SEDIMENTATION FROM PASISAR DEEP-TOW SEISMIC DATA ACQUIRED IN THE IBERIA ABYSSAL PLAIN[1]

Jean-Claude Sibuet,[2] Yannick Thomas,[2,3] Bruno Marsset,[2] Hervé Nouzé,[2] Véronique Louvel,[2,3]
Bruno Savoye,[2] and Jean-Pierre Le Formal[2]

ABSTRACT

The ocean/continent transition (OCT) of the Iberia Abyssal Plain nonvolcanic rifted margin has been intensively drilled during Leg 149 of the Ocean Drilling Program. Site 897 is located over a serpentinized peridotite ridge interpreted as the southern expression of the peridotite ridge drilled at the OCT of the Galicia Margin during ODP Leg 103. In the Iberia Abyssal Plain, the ridge is associated with a lower Miocene synsedimentary reverse fault which merges with its eastern flank. Using the recently developed Pasisar system, a near-bottom single-channel seismic profile was acquired over this ridge during the *Fluigal* cruise (July 1993). Site 897 biostratigraphic gaps are correlated with seismic unconformities identified on this high-resolution seismic profile. The mean vertical velocity within the sedimentary column at Site 897 is 1820 m/s. The major reverse fault, which develops within the synsedimentary lower Miocene front, merges with the eastern flank of the serpentinized peridotite ridge at a significant angle of about 60°. Shear has been observed on Site 897 samples collected close to the serpentinized body, both within the serpentinite breccias and the overlying claystones. Thus, the lubricant effect of serpentinite facilitates the concentration of shear along the flanks of the serpentinized peridotite ridge. We suggest that the synsedimentary reverse fault extends along the eastern flank of the ridge and across the whole brittle crust. As reverse faulting is preferentially located where serpentinized peridotite ridges exist, reverse faults located at the base of passive continental margins could generally help to locate the ocean/continent transition if the margin has undergone compression.

INTRODUCTION

The *Fluigal* cruise (July 1993) was the first scientific cruise conducted after the completion of Leg 149 (March-May 1993). An east-southeast-west-northwest deep-tow profile was collected with the Ifremer Sonar Acoustique Remorqué (SAR) deep-tow system across Sites 898, 899, 897, and anomaly J (Figs. 1, 2). The SAR is equipped with a 170-190-kHz sidescan sonar, providing a 1500 m total width of investigation (Augustin and Voisset, 1989; Farcy and Voisset, 1985), a three-component magnetometer developed for this cruise (Sibuet et al., 1995) and the Pasisar (Passager sismique du SAR) system, also operational for the first time during this cruise. The SAR deep-tow magnetic measurements have been merged with the Tobi deep-tow measurements (Whitmarsh et al., this volume) acquired by the Institute of Oceanographic Sciences along the other portion of the Leg 149 transect (Sites 901, 900, and 898; Fig. 1). Using shallow penetration probes, about 50 heat flow measurements were also collected during this cruise along the whole Leg 149 transect as part of a joint French-Canadian program (Sibuet et al., 1994a).

The purpose of this paper is to present a portion of the near-bottom single channel seismic profile acquired during this cruise in the vicinity of Site 897 and to show how data from Holes 897C and 897D are useful to "calibrate" the seismic discontinuities clearly observed on this high-resolution seismic profile. In addition, the downward continuation of a synsedimentary reverse fault along the eastern flank of the Peridotite Ridge (PR) is discussed.

[1]Whitmarsh, R.B., Sawyer, D.S., Klaus, A., and Masson, D.G. (Eds.), 1996. *Proc. ODP, Sci. Results,* 149: College Station, TX (Ocean Drilling Program).
[2]Ifremer Centre de Brest, B.P. 70, 29280 Plouzané, France. Sibuet: jcsibuet@ifremer.fr
[3]Also at EOPGS, 5 rue R.-Descartes, 67084 Strasbourg Cedex, France.

REGIONAL BACKGROUND

Two main compressive phases have been observed west of Iberia and correspond to intraplate deformations there:

1. The Pyrenean phase, which occurred in the vicinity of the North Iberia plate boundary (Sibuet et al., 1994b; Sibuet et al., 1993) between the Late Cretaceous and late Eocene, with a significant compressive event in the late Eocene (Mattauer, 1968). Such reverse faulting is mostly observed west and north of Galicia Bank.
2. The Betic compressive phase, which occurred in the vicinity of the Azores-Gibraltar plate boundary during early Miocene, and is marked by a major hiatus between seismic layers Ia and Ib (Shipboard Scientific Party, 1994); such reverse faulting (Figs. 3, 4) is observed west of Iberia (Masson et al., 1994). However, the basement relationship with this fault and the correlation between deformed and undeformed sediments are poorly established (Figs. 3, 4).

Rifting of the Iberia Abyssal Plain (IAP) continental margin occurred from Late Jurassic (150 Ma) to Barremian (130 Ma) (Whitmarsh and Miles, 1995; Whitmarsh et al., 1990; Wilson et al., 1989). At Site 897, located at the OCT, the similarity of the basement character with that of the Galicia Margin PR led Beslier et al. (1993) to propose that the basement was composed of serpentinized peridotites. A clear confirmation of this hypothesis was given by drilling results (Shipboard Scientific Party, 1994).

Continental crust as thin as 4 to 5 km (Whitmarsh et al., 1990) implies stretching factors of 6 to 7.5. For a low asthenospheric potential temperature at the time of rifting and a long duration of the episode of rifting (20 Ma), the expected volume of melt generated by adiabatic decompression (Bown and White, 1994; 1995) is negligible. As the adjacent oceanic crust is thinner (5.5 km) (Whitmarsh et al., 1990) than the normal 7-km thickness (White et al., 1992), mantle potential temperature was 50°-100°C cooler than the temperature reached during normal seafloor spreading (Horsefield et al., 1994; Whitmarsh et al., 1993). The ascent of subcontinental asthenosphere during conti-

nental breakup was so slow that sufficient heat was lost by conduction to inhibit or largely diminish melt formation (Bown and White, 1995, in press; Horsefield et al., 1994). This explains why the magma production could be reduced to almost nothing during the passive upwelling of the asthenospheric material and why, in such conditions, mantle peridotites could be emplaced through the thin veil of continental crust. Percolation of seawater through the highly fractured crust induces the process of serpentinization. In the constructional processes of PRs, serpentinization has two principal effects: lowering the density of ultramafic rocks (2.4 to 2.9 g/cm^3 at Site 637 [Boillot et al., 1987]) and acting as a lubricant (formation of talc), facilitating isostatic equilibration (Bougault et al., 1993; Charlou and Donval, 1993).

In the Iberia Abyssal Plain, we interpret the seismic feature that bounds the eastern flank of the PR down to the upper mantle (Figs. 3, 4) as a normal fault, which was active at the end of the rifting phase, during the uplift of the ridge. East and west of the PR, lower crustal velocities of 7.3 to 7.6 km/s (Whitmarsh et al., 1990) are associated with weakly serpentinized peridotites (Pinheiro, 1994). In a tensional environment, low-density serpentinized peridotite could easily ascend from lower peridotite material. Similar features have been observed east of the Galicia Margin PR and are interpreted in a similar way (Sibuet et al., 1995). Crustal normal faults bounding the PR are characterized by low friction values and are consequently good candidates for remobilization, especially under a compressive regime (Whitmarsh et al., 1993). The Pasisar profile will help to discuss this problem.

PASISAR DEEP-TOW SEISMIC

Data Acquisition

In order to obtain better seismic images in the deep ocean, Ifremer developed in 1993 a system combining the use of a conventional source operated at the sea surface with a near-bottom, towed, single-channel seismic streamer (Fig. 5). This system was designed to operate in the 200-6000-m water-depth range (Hernandez et al., 1994; Savoye et al., 1994, 1995). The choice of the seismic source (e.g., air gun, water gun, sparker) depends both on the water depth and on the expected resolution and penetration. Depending on the source frequency bandwidth and on the operating depth, four configurations are available for the streamer: eight or 10 hydrophones mounted serially 10 cm apart for high-frequency sources and six or seven groups of three hydrophones mounted serially every 2 m for low-frequency sources.

The streamer is towed by the Ifremer SAR system at about 80 m above the seafloor behind a depressor located 50 m ahead of the fish. Analog seismic data are frequency modulated and transmitted through the leading cable and digitized on board the ship by using an adapted DELPH2 system (Elics). Surface and deep-tow seismic data are recorded on the DELPH2 system, but are also processed independently and displayed in real time. Simultaneously, the 3.5-kHz mud profiler, sidescan sonar, three-component magnetometer, which are on board the SAR, and ship navigation data are recorded.

During the *Fluigal* cruise, the seismic source was a single Sodera GI 210-in^3 air gun shot every 12 seconds (s) and operated in the harmonic mode in order to get the maximum energy in the 20-120-Hz range. The streamer was used in the seven groups of three hydrophones configuration in water depth up to 5300 m.

The following SAR navigation parameters were used to deduce the geometry of the seismic acquisition system and to correct seismic sections from traveltime artifacts:

1. the immersion (depth sensor located in the towed fish);
2. the altitude (3.5-kHz SAR sub-bottom profiler);
3. the oblique distance between the ship and the SAR (acoustic transponder).

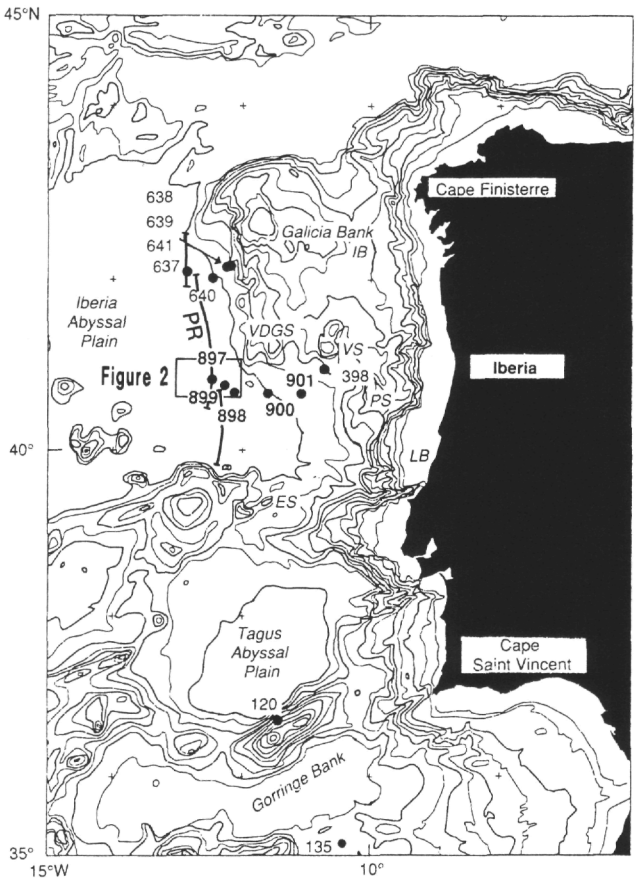

Figure 1. Location of Leg 149 Sites 897-901 and other DSDP sites along the West Iberia Margin. Location of the peridotite ridge (PR) from Beslier et al. (1993). IB = Galicia Interior Basin, VDGS = Vasco da Gama Seamount, VS = Vigo Seamount, PS = Porto Seamount, LB = Lusitanian Basin, ES = Estremadura Spur.

Specific Problems of Acquisition

To provide a reliable imagery from the sidescan sonar, the SAR has to be maintained at a constant altitude of about 80 m above the seafloor. The towing cable is therefore constantly paid in and out because of changes in the bathymetry or towing conditions. In a flat environment, the cable length could vary by several hundreds of meters to maintain the SAR at a constant altitude above the seafloor. Thus, for seismic data, reflected arrivals from the seafloor display important time shifts, which implies variations in the horizontal scale of the raw seismic line (Fig. 6).

The geometry of the acquisition system (source and receiver at different depths), implies an asymmetry of the seismic raypaths. Thus, for a given shot, the recorded seismic events do not correspond to vertical reflections from a point below the seafloor, as for conventional seismic systems, but to reflections occurring along hyperbolae (Fig. 5).

Data Processing

Standard processing procedures have been adapted in order to correct seismic sections for previous artifacts.

Conventional processing was first applied on the brute section to filter out 100 Hz and harmonic noise due to electronic problems in the pre-amplifier located in the SAR and to eliminate the direct arrival on

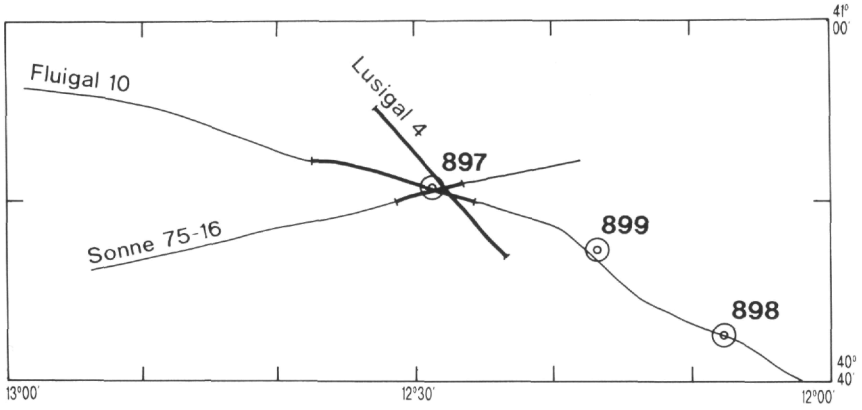

Figure 2. Sites 897, 898, and 899 locations with respect to the *Fluigal* 10 SAR deep-tow single-channel line and multichannel seismic lines *Lusigal* 4 and *Sonne* 75-16. Bold lines are portions of displayed seismic sections.

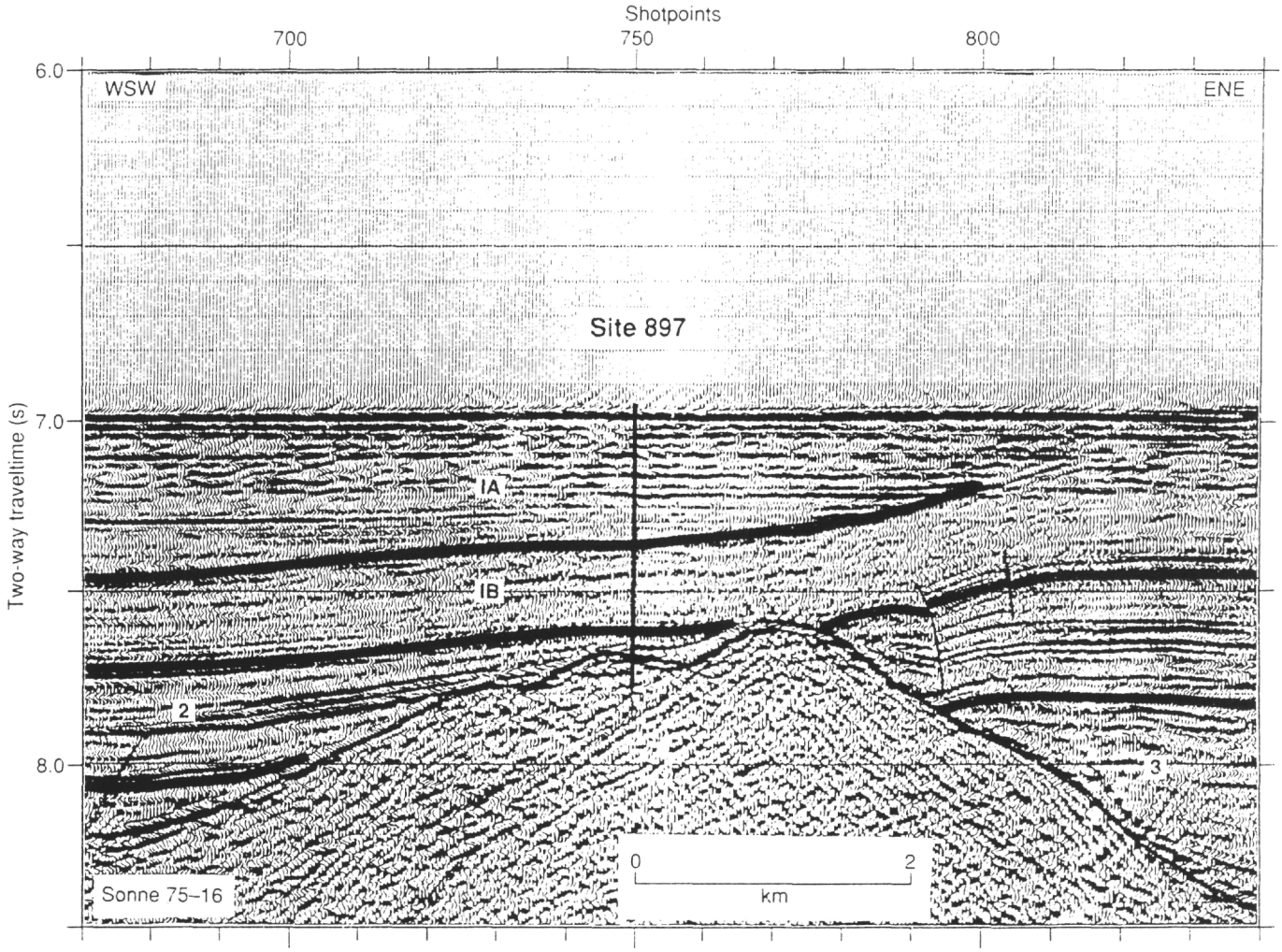

Figure 3. Portion of migrated multichannel seismic reflection profile *Sonne* 75-16 across Site 897 (Shipboard Scientific Party, 1994) and located in Figure 2.

the deep-tow streamer. Oblique linear events which appear on the seismic section (Fig. 6) come from the mud profiler operated asynchronously with respect to the seismic source. This unwanted signal was attenuated through automatic detection and subtraction.

The second step consists of calculating reliable geometrical information from the SAR navigation parameters (Fig. 7). As the angle between the towing cable and the vertical is about 30° and as the SAR is far behind the ship, the noise on navigation parameters is sometimes too large and the resulting geometry becomes of poor quality. In that case, seismic data may be used to compute the altitude and the oblique distance, by picking the first break of both sea bottom and direct arrivals.

Using this geometrical information, we can now compute a zero offset profile in depth by running a modified Kirchoff migration, which takes into account the asymmetry of the acquisition system and its geometrical configuration (Hernandez et al., 1994; Savoye et al., 1994; 1995). The reflectivity function is approximated by the correlation between the extrapolated receiver field and the propagated

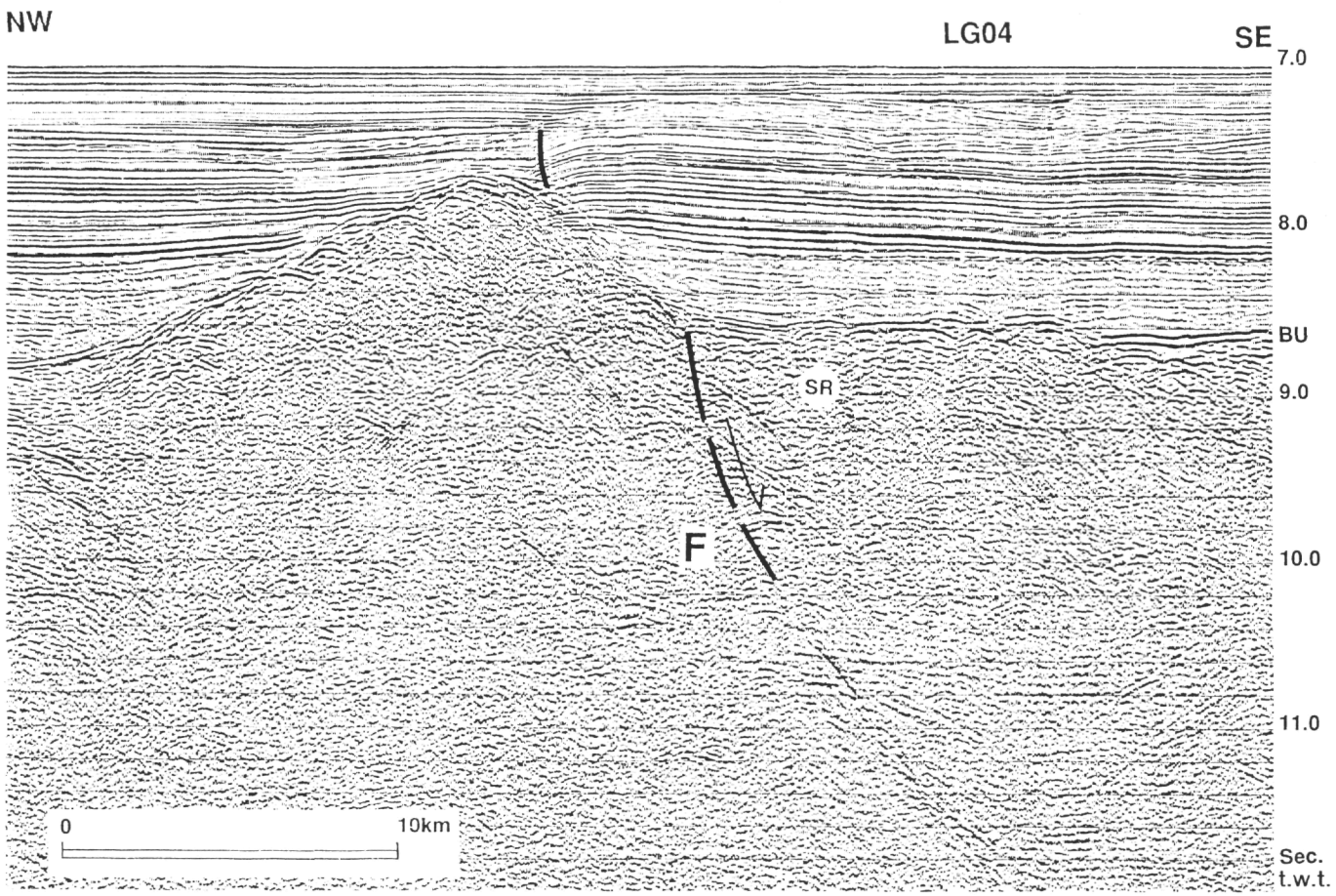

Figure 4. Portion of the stacked seismic line *Lusigal* 4 located in Figure 2 and showing the normal fault (F) bounding the PR to the east as suggested by Beslier et al. (1993). This normal fault has been reactivated as a reverse fault during lower Miocene. SR = synrift sediments; BU = breakup unconformity.

source field. The Kirchoff integral allows the calculation of these fields by assuming that:

1. the source and receiver positions are accurate enough from the previous processing of the geometric parameters;
2. the computation of first time arrivals solving the Eikonal equation is valid everywhere (Podvin and Lecomte, 1991);
3. the velocity field used for computing the first time arrivals is correct.

The migration grid is centered on the theoretical source-receiver midpoint and widened in order to take into account the asymmetry of the acquisition device. However, to reduce unwanted smoothing, data are kept only on the portion of the migration grid corresponding to a narrow migration corridor parallel and symmetrical to the location of reflection points on the hyperbola. This hyperbola represents the true location of reflection points, assuming a horizontally layered medium, and is computed using the geometrical parameters.

The migration algorithm was first tested on synthetic data. In Figure 8A, the model consists of two horizontal sedimentary layers and a sinusoidal SAR trajectory located at an mean altitude of 100 m. In this example, the Kirchoff migration we used is a robust algorithm which corrects both platform motions and drift of the reflection point with respect to the vertical (Fig. 8B, C). In addition, this type of processing may correct the imagery from slope effects (Figs. 6, 9A).

A mean velocity of 1820 m/s has been deduced from the correspondence between drilling biostratigraphic gaps and acoustic unconformities within the sedimentary cover at Site 897 (Table 1). The

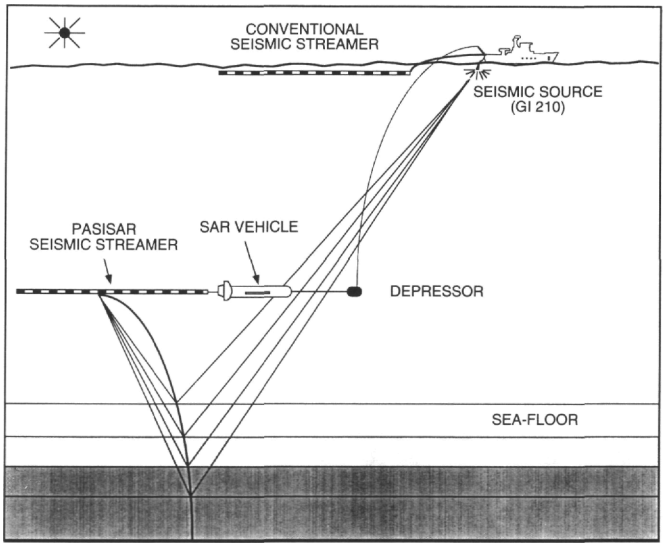

Figure 5. Scheme of the Pasisar system with the surface seismic source and the single-channel streamer towed by the SAR (sidescan sonar) at about 80 m above the seafloor. Note that for each shot, reflection points are located on a piece-wise hyperbola with its top at the SAR location.

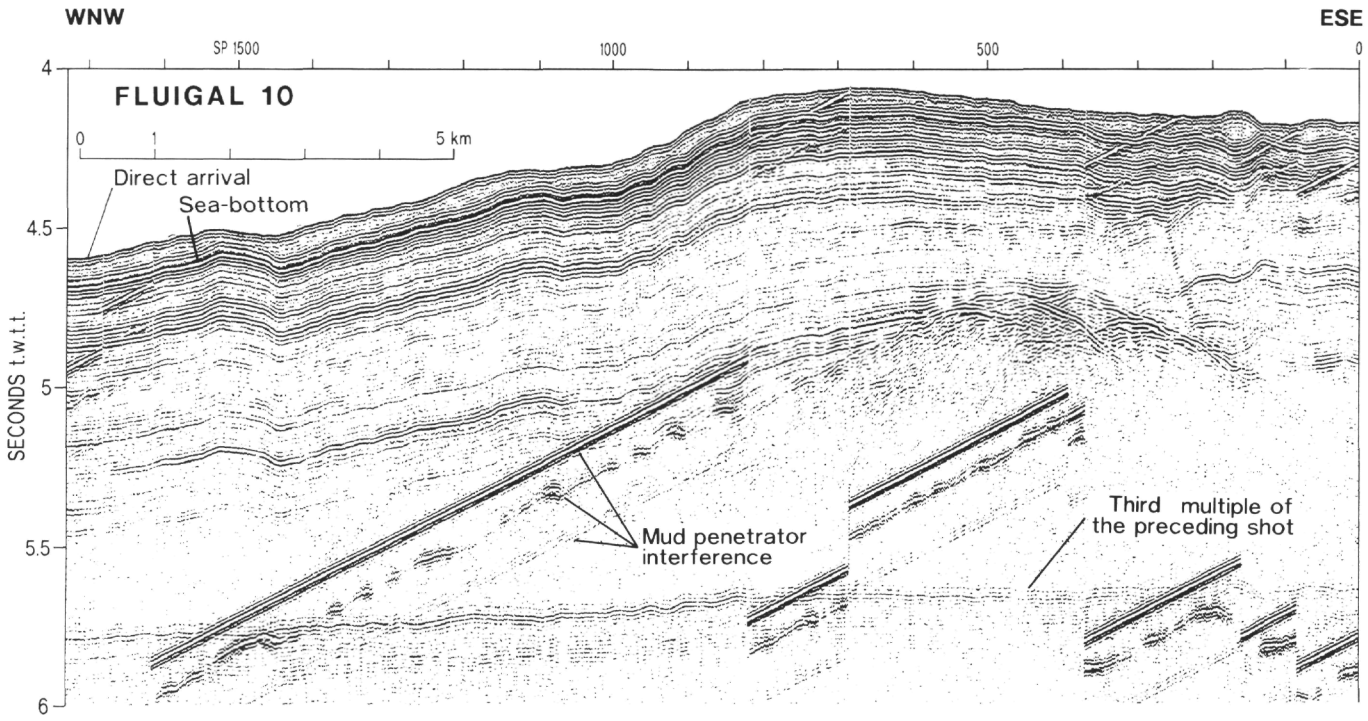

Figure 6. Filtered record section of a portion of the near-bottom *Fluigal* single-channel profile 10 located in Figure 2. Shots every 12 s with a speed of the SAR about 1.5 knots. Vertical scale in seconds. The first arrival is the direct arrival. About 0.1 s below is the sea-bottom reflection. Linear oblique stripes correspond to SAR mud penetrator interferences. To avoid interactions within the first second of the useful recording sequence, they were manually offset on the ship by shifting the shooting sequence. Though the sea bottom is flat, the traveltime of the direct arrival, which varies from 4.1 to 4.6 s, is a function of the cable length of the SAR. The cable length is adjusted in order to maintain the SAR at about 80 m above the seafloor but depends on such factors as weather, currents, or the speed of the ship. The arrival at about 5.75 s is the third conventional multiple of the preceding shot.

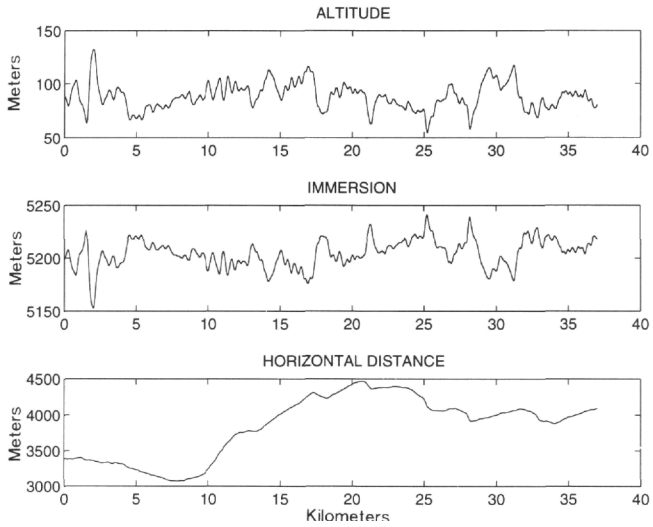

Figure 7. Altitude, immersion (depth), and horizontal distance of the SAR to the ship as functions of distance along traverse.

field data were processed by using a two-dimensional velocity model, in which the mean velocity within the sediments is 1820 m/s, and only a three-trace-wide migration corridor to avoid data smoothing. Thus, the so-called migrated profile should be geometrically corrected, but some diffraction hyperbolae were not sufficiently collapsed (Fig. 9A). Assuming that the obtained depth section was accurate, we could time convert it back to a zero offset time profile, using the velocity field of this first "Kirchoff-like migration."

Then, we could apply a Kirchoff depth migration, using multiple arrival ray tracing, to cope with hyperbolic diffractions. The first two-dimensional velocity model (1820 m/s) was then fitted with regards to the migration results. These velocities were then adjusted by successive trials in order to get the best section which displays the minimum diffraction energy. The final chosen interval velocities are 1820 m/s in the sediments, 2000 m/s at the interface between the sediments and the PR basement over a 50-m-thick layer, and 2200 m/s below. With these velocities, the diffraction energy seems to be better stacked and the contacts between the sediments and the basement are better defined on the final migrated section (Fig. 10).

SEISMIC CALIBRATION

The final processed sections display much more information than was expected onboard the ship for this first trial in deep waters. With respect to conventional MCS data (Figs. 3,4), the deformed sedimentary sequence as well as an internal reverse fault are more clearly imaged (Figs. 9A, B). Note that the upper 200 m of the serpentinized ridge displays acoustic reflectors (Fig. 10). These reflectors could be explained by seawater circulation and subsequent variations in the degree of serpentinization, as well as by the presence of breccias and debris-flow deposits at Sites 897 and 899, composed of peridotite and sediments (Shipboard Scientific Party, 1994). One of the main problems is always to correlate site observations with seismic data. As no downhole velocity logs were obtained at Site 897, it is not possible to directly correlate reflectors seen on seismic reflection profiles and acoustic impedance and reflection coefficients computed from physical measurements (Shipboard Scientific Party, 1994).

Based on onlap identifications (Fig. 9B), four seismic unconformities have been recognized on the Pasisar profile at depths of 170,

310, 350, and 525 m at the Site 897 location (Table 1). The acoustic unconformities at 170, 310, and 525 m are of minor importance but the one at 350 m corresponds to the disappearance of a significant portion of sediments at the base of a sedimentary section which seems to be rather complete at shotpoint (SP) 1100 (Fig. 9B). At the western end of the seismic section, unconformities at 310 and 350 m merge to become nearly single.

Holes 897C and 897D are 100 m apart and offset by less than 500 m from the *Fluigal* seismic line. Table 1 shows the correlation between the identified seismic unconformities and the biostratigraphic gaps, except for the deeper unconformity that corresponds to the contact of sediments with the ridge. This correlation is the best for a mean velocity of 1820 m/s. From the velocity-depth profile at the DSDP Site 398, the velocity is 1820 m/s in the upper 400 m (Shipboard Scientific Party, 1979) and 1850 and 1860 m/s from two sonobuoy experiments conducted in the vicinity of Site 897 (Whitmarsh et al., 1990).

The second important point is that the lower Miocene deformation front associated with the Betic tectonics is located at SP 390 and is clearly displayed on the Pasisar high-resolution seismic profile (Figs. 6, 9). Seismic reflectors are continuous from the undeformed to the deformed areas. The top of the deformed zone clearly merges with the lower Miocene discontinuity and the upper Eocene-lower Oligocene unconformity can be continuously followed through the deformed zone (Figs. 6, 9). Below this unconformity, the significant change in the slope of sedimentary layers at SP 900-1000 is probably related to the Pyrenean compressive phase with the presence of a fault merging with the western PR flank. A clearly defined synsedimentary reverse fault with less than a few meters vertical offset appears at SP 300. Furthermore, as the deformation front is parallel to this major reverse fault, it could correspond to the initiation of a second reverse fault with an almost zero vertical offset, which merges at the top of the PR.

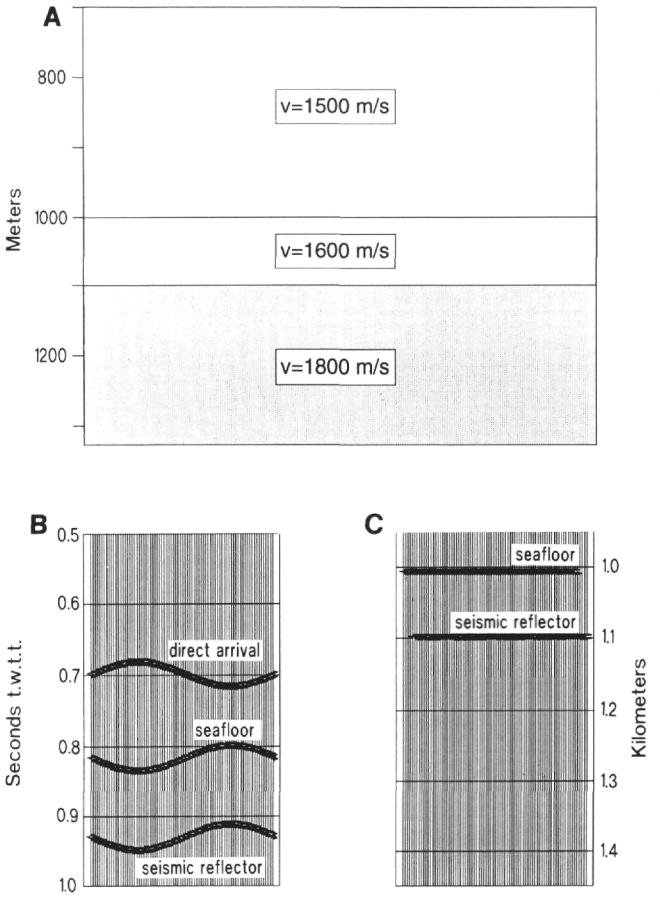

Figure 8. **A**. Model with two horizontal layers. **B**. Synthetic seismogram with the direct arrival corresponding to a sinusoidal SAR trajectory located at a mean altitude of 100 m above the seafloor. **C**. Geometrical correction of the synthetic profile.

ROLE OF SERPENTINIZED PERIDOTITES DURING THE MIOCENE COMPRESSION

The main reverse fault (at SP 390) intersects the PR at a significant angle of about 60° (Fig. 9B). In the portion of the sedimentary section located east of the ridge and below the depth of the intersection point of the reverse fault and the ridge, sedimentary layers are flat (SP 0-200). This implies that the eastern prolongation of the major reverse fault occurs along the contact between the PR and the sedimentary cover (Fig. 11).

We propose a model of crustal and sedimentary compressive deformation focused by the presence of a serpentinized PR, in which the basic intraplate compressive motion occurs along a main intracrustal fault, accommodating the crustal shortening within the brittle crust (Fig. 11). In fact, the compressive motion could correspond to the reactivation of a large normal fault (Fig. 4), which limits the PR and was active at the end of rifting during the uplift of the ridge as suggested by Beslier et al. (1993). This crustal fault probably separates the lower crustal serpentinized peridotites already evidenced from refraction measurements (Pinheiro, 1994; Whitmarsh et al., 1990) from the highly serpentinized peridotites that compose the ridge. In addition, the seawater circulation might increase the degree of serpentinization along the fault and, consequently, the formation of lubricant (e.g., clay or talc) and the probability of further reverse motion along it. During the Betic compression, the reverse fault follows the interface between the ridge and the sediments already deposited up to the top of the ridge. Sediments infilling depressions remain undisturbed. However, sediments lying above the ridge are deformed and the portion of the reverse fault located within the sediments merges with the sea bottom of that time. The dip of the reverse fault is a function of the physical properties of the sediments, which explains why the fault trend makes a significant angle of about 60°, with the portion of the fault lying along the ridge flank. West of the main reverse fault, the deformation front corresponds to a very small reverse fault, which implies a slight shear motion near the top of the ridge.

The existence of a normal fault that was reactivated as a reverse fault during the Betic orogeny is supported by ODP drilling results. Within Holes 897C and 897D, 180 m of clayey conglomerates with serpentinite, sandstone, dolomite, limestone, claystone with serpentinite, massive serpentinized peridotite with shear bands have been drilled (Shipboard Scientific Party, 1994). Site 897 peridotites underwent a late shear deformation event, leading to the development of foliation and shear bands in the serpentinite and local brecciation of the serpentinite. These tectonic breccias occur throughout the cores of both holes and are locally extremely sheared or fractured. The shear features may document a deformation involving the upper portion of the basement during the last stages of rifting that may have trapped sediments within the shear zone. Site 897 is located west of the deformation front. No sign of Tertiary shear motion appears in the cores. However, both the extensively serpentinized upper portion of the ultramafic section and the underlying claystone with serpentinite breccias are appropriate candidates for the location of shear motion as suggested by the model.

Peridotites emplaced at the OCT are characterized by a high degree of serpentinization (Girardeau et al., 1988). Because the process of serpentinization results in a lubricant effect, PRs emplaced at the OCT are potentially weak zones for further tensional or compressive

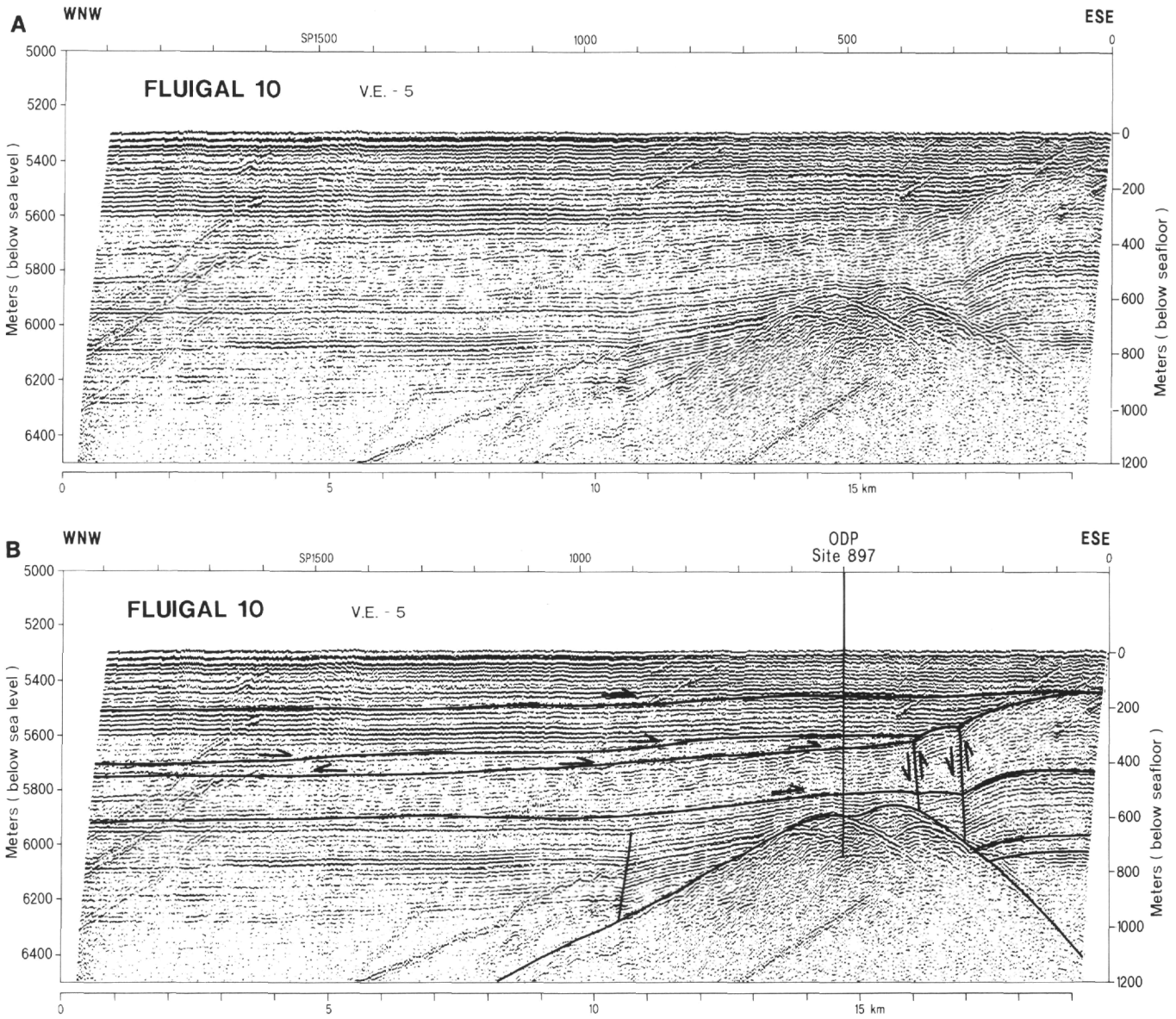

Figure 9. **A.** "Kirchoff-like" migrated section of a portion of the near-bottom *Fluigal* single-channel profile 10 shown in Figure 6. Processing was completed with a velocity of 1820 m/s in the sediments. Vertical scale in meters. Vertical exaggeration is 5. The seafloor is flat. **B.** Seismic discontinuities and faults are displayed on the section. Location of Site 897, offset about 500 m from the line, has been projected on the seismic section. Reverse faulting on the eastern side of the ridge is linked to the Betic compressive phase and on the western side of the ridge to the Pyrenean compressive phase. Arrows indicate onlaps which help to define the four seimic unconformities identified in the sedimentary sequence (Table 1).

Table 1. Correspondence between drilling biostratigraphic gaps and acoustic unconformities at Site 897, assuming a 1820 m/s mean velocity in the sediments.

Biostratigraphic gaps at Site 897 (mbsf)	Duration of biostratigraphic gap (Ma)	Age of biostratigraphic gaps (Ma and period)	Depth of seismic unconformities (mbsf)
175	2	2–4, Pliocene	170
300	4	4–8, late Miocene/early Pliocene	310
342	7	18–25, early Miocene	350
525	2	34–36, late Eocene/early Oligocene	525
625	62?	48–110?, middle Eocene	605

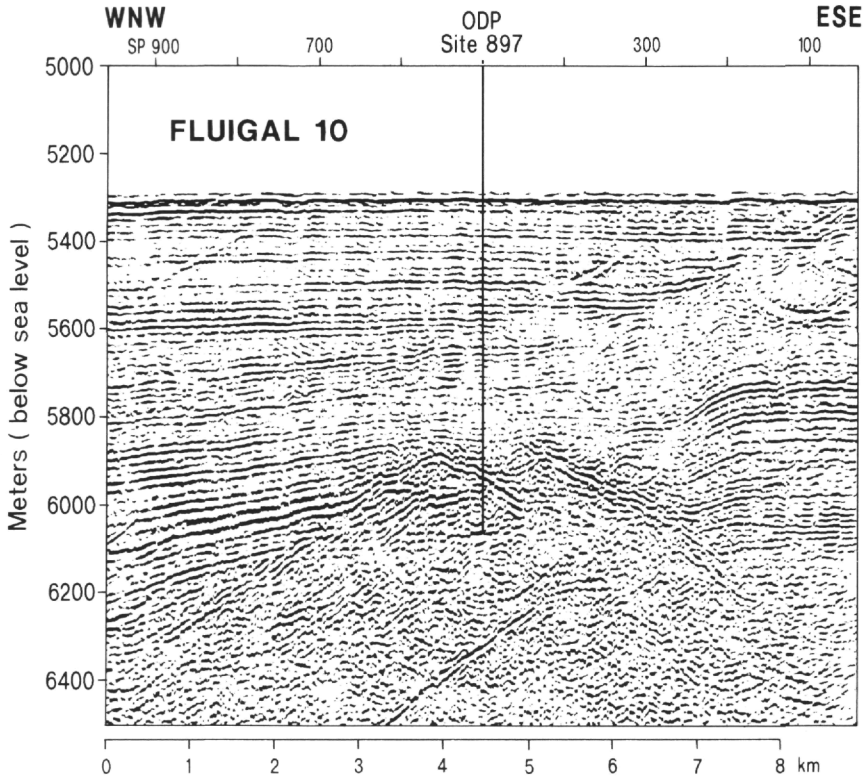

Figure 10. Migrated section of a portion of the corrected profile shown in Figure 9A (Kirchoff depth migration using the multiple-arrival ray-tracing method with a vertically and laterally variant interval velocity field in depth). Note that the shape of the PR basement seems to be correctly restored and that diffraction hyperbolae are removed. In addition, sedimentary acoustic reflectors disappear just at their contact with the basement. However, the reverse fault is poorly imaged by this type of processing.

motions. Strain deformations will be primarily localized along the PR flanks. Therefore, under significant compressive motion, the final result could be the duplication of transitional crust and the formation of Ophiolites as suggested by Whitmarsh et al. (1993).

Seismic profiles acquired in the Iberia Abyssal Plain show that up to two parallel reverse faults exist there (Beslier et al., 1993; Whitmarsh and Miles, 1995). This may mean that two overlapping PRs lie parallel to the margin and correspond to uplifted portions of lower crustal peridotite with highly serpentinized material at their surface. However, the absence of serpentinized ridges does not mean that a lower crustal peridotite layer is absent, as attested by refraction results obtained west of Iberia on the Galicia Margin (Horsefield, 1992; Sibuet et al., 1995; Whitmarsh et al., 1993), Iberia Abyssal Plain margin (Pinheiro, 1994; Whitmarsh et al., 1990), and Tagus Abyssal Plain margin (Pinheiro, 1994; Pinheiro et al., 1992), but this only means that no PR has been uplifted during the last stages of rifting of these continental margins.

This statement is only valid in faint compressive settings such as the Betic, west of Iberia. It is anticipated that for larger compressive motions, as in the north Galicia area during the Pyrenean phase of compression, reverse faults could also develop along previous zones of weakness, as well as along normal faults that were previously active during rifting and that bound tilted fault blocks located over extremely thinned continental crust.

In a reverse manner, the existence of a slight compressive motion could help to locate the OCT, if serpentinized PRs are present. PRs probably exist in the Tagus Abyssal Plain, for example, where refraction and magnetic data are insufficient to precisely locate the OCT (Pinheiro, 1994). Here, well defined synsedimentary reverse faulting has been observed on several seismic profiles acquired in this area. We suggest that these Miocene reverse faults are associated with a crustal motion that occurs along serpentinized PRs emplaced at the OCT. However, further geophysical work is needed to confirm such a hypothesis.

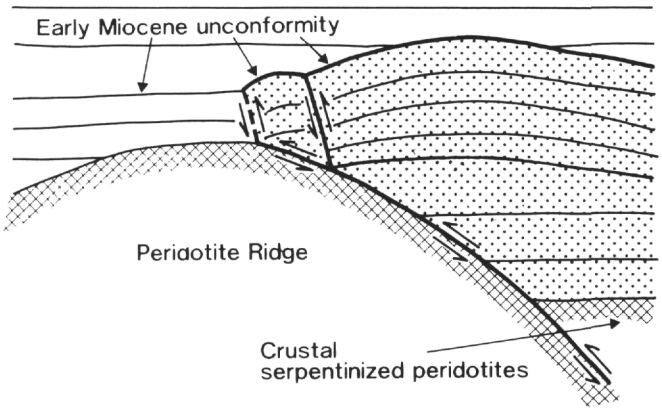

Figure 11. Scheme of crustal and sedimentary compressive deformation focused by the presence of a serpentinized peridotite ridge. The prolongation of the major synsedimentary reverse fault occurs along the contact between the serpentinized PR and the sedimentary cover. Dotted areas correspond to sediments deformed during the Betic compressive phase.

CONCLUSIONS

Based on the acquisition of a deep-tow seismic profile calibrated at Site 897, we have clearly imaged reverse faulting associated with the existence of a serpentinized PR located within the OCT zone. The main conclusions of this study are:

1. The Pasisar deep-tow seismic system is a useful tool to image deep seismic features such as acoustic sedimentary sequences and tectonic features.

2. Seismic unconformities calibrated with Site 897 biostratigraphic unconformities allow us to define a mean vertical velocity in the sedimentary column of 1820 m/s.

3. The major reverse fault that develops within the synsedimentary Miocene deformation zone merges with the eastern flank of a serpentinized PR identified by drilling.

4. Site 897 cores show that the surface of the PR underwent a late shear deformation event. As the process of serpentinization facilitates a lubricant role, we suggest that the synsedimentary reverse fault has a downward prolongation along the eastern flank of the PR and within the whole brittle crust.

5. As reverse faulting is preferentially located where serpentinized PRs exist, reverse faults located at the base of passive continental margins could help to recognize and locate the OCT, as in the Tagus Abyssal Plain.

ACKNOWLEDGMENTS

We thank the Ifremer Engineering Department and Pierre Plasseraud and Pierre Léon (technical staff in charge of the SAR) for their help in the development and integration of the Pasisar system in the SAR. Thanks to the SAR and seismic operational team, the Pasisar was tested and became operational during its first cruise. We thank the master and crew of the *Le Suroît* and the *Fluigal* scientific party for their help at sea under difficult conditions. We thank Roger Searle and Bob Whitmarsh for their constructive reviews and an anonymous reviewer who pointed out some major problems about our preliminary processing of the Pasisar data. We thank G. Lericolais for his help and advice on using the seismic processing software Sithere, and D. Carré for drafting the figures.

REFERENCES

Augustin, J.-M., and Voisset, M., 1989. Images sonar et cartographie en géologie. *L'Onde Electr.,* 69:20-27.

Beslier, M.-O., Ask, M., and Boillot, G., 1993. Ocean-continent boundary in the Iberia Abyssal Plain from multichannel seismic data. *Tectonophysics,* 218:383-393.

Bougault, H., Charlou, J.L., Fouquet, Y., Needham, H.D., Vaslet, N., Appriou, P., Baptiste, P.J., Rona, P.A., Dmitriev, L., and Silantiev, S., 1993. Fast and slow spreading ridges: structure and hydrothermal activity, ultramafic topographic highs, and CH_4 output. *J. Geophys. Res.,* 98:9643-9651.

Bown, J.W., and White, R.S., 1994. Variation with spreading rate of oceanic crustal thickness and geochemistry. *Earth Planet. Sci. Lett.,* 121:435-449.

———, 1995. Finite duration rifting, melting and subsidence at continental margins. *In* Banda, E., Torné, M., and Talwani, M. (Eds.), *Rifted Ocean-Continent Boundaries,* NATO ASI Series E: Mathematical and Physical Sciences, 463:31-54.

———, in press. The effect of finite extension rate on melt generation at continental rifts. *J. Geophys. Res.*

Charlou, J.-L., and Donval, J.-P., 1993. Hydrothermal methane venting between 12°N and 26°N along the mid-Atlantic ridge. *J. Geophys. Res.,* 98:9625-9642.

Farcy, A., and Voisset, M., 1985. Acoustic imagery of sea floor. *In* Anderson, V.C. (Ed.), *Oceans '85: Ocean Engineering and the Environment* (Vol. 2): New York (IEEE), 1005-1012.

Girardeau, J., Evans, C.A., and Beslier, M.-O., 1988. Structural analysis of plagioclase-bearing peridotites emplaced at the end of continental rifting: Hole 637A, ODP leg 103 on the Galicia Margin. *In* Boillot, G., Winterer, E.L., et al., *Proc. ODP, Sci. Results,* 103: College Station, TX (Ocean Drilling Program), 209-223.

Hernandez, F., Marsset, B., Savoye, B., De Roeck, Y.H., Meunier, J., and Lopes, L., 1994. Pasisar: processing of very high-resolution near-bottom seismic data. In *Oceans '94: Oceans Engineering for Today's Technology and Tomorrow's Preservation* (Vol. 2): New York (IEEE), 665-670.

Horsefield, S.J., 1992. Crustal structure across the continent-ocean boundary [Ph.D. thesis]. Cambridge Univ.

Horsefield, S.J., Whitmarsh, R.B., White, R.S., and Sibuet, J.-C, 1994. Crustal structure of the Goban Spur rifted continental margin, NE Atlantic. *Geophys. J. Int.,* 119:1-19.

Masson, D.G., Cartwright,J.A., Pinheiro, L.M., Whitmarsh, R.B., Beslier, M.-O., and Roeser, H., 1994. Compressional deformation at the ocean-continent transition in the NE Atlantic. *J. Geol. Soc. London,* 151:607-613.

Mattauer, M., 1968. Les traits structuraux essentiels de la chaîne Pyrénéenne. *Rev. Geol. Dyn. Geogr. Phys.,* 10:3-11.

Pinheiro, L.M., 1994. The crustal structure under the Tagus Abyssal Plain and the ocean-continent transition off western Iberia [Ph.D. thesis]. Univ. London.

Pinheiro, L.M., Whitmarsh, R.B., and Miles, P.R., 1992. The ocean-continent boundary off the western continental margin of Iberia, II. Crustal structure in the Tagus abyssal plain. *Geophys. J. Int.,* 109:106-124.

Podvin, P., and Lecomte, I., 1991. Finite difference computation of travel times in very contrasted velocity models: a massively parallel approach and its associated tools. *Geophys. J. Int.,* 105:271-284.

Savoye, B., Léon, P., De Roeck, Y.H., Marsset, B., Lopes, L., and Hervéou, J., 1994. Pasisar: a new tool for near-bottom seismic profiling in deep water. In *Oceans '94: Oceans Engineering for Today's Technology and Tomorrow's Preservation* (Vol. 1): New York (IEEE), 652-657.

———, 1995. Pasisar: a new tool for near-bottom very high-resolution profiling in deep water. *First Break,* 13:253-258.

Shipboard Scientific Party, 1979. Site 398. *In* Sibuet, J.-C., Ryan, W.B.F., et al., *Init. Repts. DSDP,* 47 (Pt. 2): Washington (U.S. Govt. Printing Office), 25-233.

———, 1994. Site 897. *In* Sawyer, D.S., Whitmarsh, R.B., Klaus, A., et al., *Proc. ODP, Init. Repts.,* 149: College Station, TX (Ocean Drilling Program), 41-113.

Sibuet, J.-C., Louden, K.E., and Mareschal, J.-C., 1994a. Measurements of heat flow and radiogenic heat production from the Iberia basin along the ODP 149 transect. *Eos,* 75:616.

Sibuet, J.-C., Louvel, V., Whitmarsh, R.B., White, R.S., Horsefield, S.J., Sichler, B., Léon, P., and Recq, M., 1995. Constraints on rifting processes from refraction and deep-tow magnetic data: the example of the Galicia continental margin (West Iberia). *In* Banda, E., Torné, M., and Talwani, M. (Eds.), *Rifted Ocean-Continent Boundaries,* NATO ASI Series C: Mathematical and Physical Sciences, 463:197-217.

Sibuet, J.-C., Monti, S., and Pautot, G., 1994b. New bathymetric map of the Bay of Biscay. *C. R. Acad. Sci.,* 318:615-625.

Sibuet, J.-C., Monti, S., Réhault, J.-P., Durand, C., Gueguen, E., and Louvel, V., 1993. Quantification de l'extension liée à la phase pyrénéenne et géométrie de la frontière de plaques dans la partie ouest du golfe de Gascogne. *C. R. Acad. Sci.,* 317:1207-1214.

White, R.S., McKenzie, D., and O'Nions, R.K., 1992. Oceanic crustal thickness from seismic measurements and rare earth element inversions. *J. Geophys. Res.,* 97:19683-19715.

Whitmarsh, R.B., and Miles, P.R., 1995. Models of the development of the West Iberia rifted continental margin at 40°30'N deduced from surface and deep-tow magnetic anomalies. *J. Geophys. Res.,* 100:3789-3806.

Whitmarsh, R.B., Miles, P.R., and Mauffret, A., 1990. The ocean-continent boundary off the western continental margin of Iberia, I. Crustal structure at 40°30'N. *Geophys. J. Int.,* 103:509-531.

Whitmarsh, R.B., Pinheiro, L.M., Miles, P.R., Recq, M., and Sibuet, J.-C., 1993. Thin crust at the western Iberia ocean-continent transition and Ophiolites. *Tectonics,* 12:1230-1239.

Wilson, R.C.L., Hiscott, R.N., Willis, M.G., and Gradstein, F.M., 1989. The Lusitanian Basin of west-central Portugal: Mesozoic and Tertiary tectonic, stratigraphic and subsidence history. *In* Tankard, A.J., and Balkwill, H.R. (Eds.), *Extensional Tectonics and Stratigraphy of the North Atlantic Margins.* AAPG Mem., 46:341-361.

Date of initial receipt: 5 December 1994
Date of acceptance: 28 June 1995
Ms 149SR-248